IEEE Access
Multidisciplinary | Rapid Review | Open Access Journal

Received March 16, 2020, accepted April 26, 2020, date of publication April 29, 2020, date of current version May 15, 2020.

Digital Object Identifier 10.1109/ACCESS.2020.2991381

Load-Aware Energy Efficient Adaptive Large Scale Antenna System

WAHYU PRAMUDITO[1], (Member, IEEE), EMAD ALSUSA[1], (Senior Member, IEEE), ARAFAT AL-DWEIK[2,3], (Senior Member, IEEE), KHAIRI A. HAMDI[1], (Senior Member, IEEE), DANIEL K. C. SO[1], (Senior Member, IEEE), AND THOMAS L. MARZETTA[4], (Life Fellow, IEEE)

[1]School of Electrical and Electronic Engineering, University of Manchester, Manchester M13 9PL, U.K.
[2]Center for Cyber Physical Systems (C2PS), Khalifa University, 127788 Abu Dhabi, UAE
[3]Department of Electrical and Computer Engineering, Western University, London, ON N6A 5B9, Canada
[4]Department of Electrical and Computer Engineering, New York University, New York, NY 10003, USA

Corresponding author: Emad Alsusa (e.alsusa@fmanchester.ac.uk.org)

This work was supported by the European Union's Horizon 2020 Research and Innovation Programme under Grant 812991.

ABSTRACT This paper proposes an adaptive large scale antenna system (ALSAS) for enhancing energy efficiency in low density wireless network scenarios. The proposed ALSAS comprises of two stages, a novel adaptive discontinuous transmission (ADTx) stage and an antenna array optimization (AAO) one. The basic idea is to utilize prior knowledge of the users' quality of service (QoS) requirements as well as precoding selection in the ADTx stage to maximize the transmitter hibernation periods subject to a certain complexity constraint. In the AAO stage, further power saving is achieved by reducing the number of active antenna elements subject to a certain QoS requirement. It is shown that, relative to conventional large scale antenna system (LSAS), the proposed ALSAS system achieves significant energy efficiency improvements under various scenarios. The results show that the proposed technique can provide energy efficiency improvement between 125% and 1124% in the suburban scenario, and between 196% and 952% in the rural scenario. It is also demonstrated that for rural environments with relatively small short inter-site-distance (ISD) values, ALSAS can provide up to 500% power saving for the fixed bit rate requirement case.

INDEX TERMS Massive MIMO, discontinuous transmission, adaptive precoding energy efficiency, QoS, suburban and rural scenarios.

I. INTRODUCTION

It is well-known that multiple-input multiple-output (MIMO) technology can significantly increase the network capacity through spatial multiplexing [1]. The fifth generation (5G) New Radio (NR) standard supports a single user equipment (UE) in single-user MIMO with a maximum of eight antennas for the down link (DL) and four for the uplink (UL) [2, pp. 29]. It also supports multi-antenna data transmission for multiple UEs, multi-user MIMO, with a maximum of twelve transmission layers for the DL and UL. MIMO, in the form of large scale antenna system (LSAS), or massive MIMO, is used as a multiuser multiplexing technique for its ability to satisfy the growing demands in wireless networks. In fact, having a large number of antennas does not only allow increasing the number of multiplexed users, but it also reduces the channel variation across the spectrum making the channel response flat which could increase the achievable capacity [3], [4]. Furthermore, beamforming in LSAS reduces the interference for the cell-edge users and allows full spectrum utilization without soft frequency reuse as in the Long Term Evolution (LTE) standard [5]. Another advantage of LSAS is the reduced isotropic radiated power (EIRP) per antenna, which simplifies the antenna chain design and lowers the power consumption per antenna chain [6]. That is, each LSAS antenna can employ a radio frequency (RF) chain similar to that of a small cell with a more efficient power amplifier (PA), orthogonal frequency division multiplexing (OFDM) modulator, low noise amplifier (LNA), etc. For instance, a small cell PA can have 50% power efficiency compared to 25% in a conventional macro base station (MBS) [7]. Several practical demonstrations have confirmed the tremendous advantage of LSAS. For example, Samsung's 64×64 massive MIMO test revealed a 640% peak throughput improvement compared to a 4×4 MIMO [8].

The associate editor coordinating the review of this manuscript and approving it for publication was Di Zhang.

The combination of low power consumption and high achievable throughput is what makes LSAS an ideal technology for 5G networks. This is especially true for a high user-density scenario where the number of multiplexed users is large. On the other hand, in low density environments, such as off-peak urban, suburban and rural scenarios, a large number of antennas may become counterproductive [7], [9]. Therefore, energy efficiency (EE) improvement will lead to a significant power reduction [7]. One way to achieve high EE using LSAS is by taking into account the general behavior of the UEs. As shown in [10], more than 40% of mobile cellular traffic is used for low data rates such as e-mail, short messages and voice over Internet protocol (VoIP), which usually require a bit rate of less than 1.5 Mbps. Although the remaining 60% of the traffic corresponds to video, most live video streaming applications require less than 0.5 Mbps for both watching and broadcasting [11]. Therefore, a full buffer scenario is not common for most cases, making discontinuous transmission (DTx) [12] an effective tool to improve EE in low density LSAS networks. DTx was originally used to reduce interference in communication channels [13], and later for reducing power consumption in LTE [14]–[19], by regularly putting a certain base station in hibernation mode. It is shown in [14] that significant power saving can be achieved when the traffic load is low. Most existing work on DTx considers wireless systems with a small number of antennas, and employ interference and transmission coordination [20]. To the best of the authors' knowledge, DTx has never been incorporated into LSAS. The closest implementation of DTx in a system with a large number of antennas is in massive distributed antenna system [21].

In addition to DTx, extensive work has been invested to optimize the EE in LSAS. In general, such metric can be optimized using well-known techniques such as the Dinkelbach and fractional programming algorithms [22], [23]. For example, Fang *et al.* [24] proposed a solution to a non-convex optimization problem with nonorthogonal multiple access (NOMA) by using constraints that include the outage probability. In [25] the authors addressed maximizing the EE subject to specific power and data rate constraints, while in [26] the authors claimed to achieve near-optimal EE using joint antenna selection, power optimization and user selection. In [27] a low-complexity EE optimization solution based on maximum transmitted power and minimum data rate constraint is proposed based on fractional programming, learning, and game theory. Other works focused on the user association and/or power allocation such as [28], [29]. Given the aforementioned discussion, reducing the power consumption in wireless networks under low density scenarios is indispensable. Therefore, by capitalizing on our work [30]–[32], we propose an adaptive LSAS (ALSAS) technique that utilizes a combination of a novel adaptive DTx (ADTx) combined with precoding selection. The proposed ADTx exploits the quality of service (QoS) information, such as bit rate and latency requirements, and the flexibility of switching between different precoding techniques to maximize the antennas hibernation periods. Although there are many precoding techniques to choose from, such as conjugate beamforming (CJ), zero forcing (ZF), minimum mean square error (MMSE), and dirty paper precoding [33], [34], we confine the choice here to ZF and CJ, which are prominent precoding techniques [4]. It is worth noting that ZF has lower complexity than MMSE while can also provide near-optimal sum rate when the number of antennas is much larger than the number of users [35, pp. 67], which is the case in this paper. While CJ offers low complexity at the expense of some performance degradation when the number of users is relatively large, ZF trades complexity for improved performance when the number of users is large. After the ADTx stage, ALSAS performs antenna array optimization (AAO) to increase the hibernation period and achieve additional transmission power reduction. It will be shown that the proposed technique significantly improves EE in LSAS systems, especially when the network load is low, in both suburban and rural scenarios, while satisfying the QoS. Furthermore, the proposed technique provides a significant EE improvement when the cell size is reduced. To validate our claims, mathematical analysis corroborated by simulation results are presented for several use cases of interest. As compared to [30]–[32], this paper extends and refines the DTX scheme to a full adaptive one and tailors its optimization to low density sub-urban and rural scenarios. Additionally, it includes both analytical and simulation results and extends the results and discussion sections to include various parameters of interests such as spectral efficiency and outage probability, in addition to the EE enhancement achieved in different environments

The rest of the paper is organized as follows. First, the system model and basic concepts are described in Section II. The proposed ALSAS is explained in Section III. ADTx is analyzed and evaluated in Section IV. Numerical results and conclusions are drawn in Sections V and VI, respectively.

A. SYMBOLS AND NOTATIONS

The following notations are used throughout this paper:

- Bold Upper cases and Greek letters with a bar such as $\bar{\mathbf{A}}$ and $\bar{\boldsymbol{\mathcal{A}}}$, lower case and Greek letters such as $\mathbf{a}$ and $\boldsymbol{\alpha}$ denote vectors (sets) with elements A_i, $\mathcal{A}_i$, a_i, and α_i, respectively.
- Bold upper case letters such as $\mathbf{B}$ denote matrices with elements $B_{m,n}$, where m denotes the row number and n denotes the column number. The lth row or column in $\mathbf{B}$ is denoted as $\mathbf{B}_l$.
- The unit step function $\mathrm{U}(a,b) = 1$ if $b > a$, and 0 otherwise.
- $[x]$, $\lceil x \rceil$ and $\lfloor x \rfloor$ denote the round, ceiling and floor functions, respectively.
- Subscript G and Z indicate the CJ and ZF precoding techniques, respectively.
- l is the scheduled transmission index.
- k is the user index.
- $(\cdot)^T$ is the transpose.

TABLE 1. List of abbreviations in alphabetical order.

Abbreviation	Description
ADTx	Adaptive Discontinuous Transmission
AAO	Antenna Array Optimization
CJ	Conjugate Beamforming
DTx	Discontinuous Transmission
EE	Energy Efficiency
PO	Precoder Observation
RT	Release Time
RB	Resource Block
ST	Scheduled Transmission
SE	Spectral Efficiency
ZF	Zero Forcing

TABLE 2. List of symbols.

Sym.	Description	Sym.	Description
α	Pathloss	Y	Latency duty cycle requirement
P_T	Transmitted power	K	Total number of users
T_A	Active transmission period per frame (sec.)	$R^{\max}$	Achievable bit rate for each OFDM symbol
F	Number of OFDM symbols per frame	$\boldsymbol{\mathcal{A}}$	Allocated RBs matrix
M	Total number of Tx antennas	L	Total STs
$\mathcal{M}$	Number of instantaneous antennas for the ADTx	ℓ	Pilot sequence length
ψ	SINR per antenna	$\mathcal{N}$	Number of allocated RBs
γ	SINR using precoding	S	Available OFDM symbols
R	Bit rate requirement	$\mathcal{K}$	Maximum number of multiplexed UEs
$\mathcal{E}$	Energy efficiency	$\mathcal{S}$	Allocated symbols for the ADTx
U	Unit-step function	I	Interference
$\mathbb{I}$	Set of integer numbers	$\mathbb{R}$	Set of real numbers
$\mathbb{B}$	Set of Binary numbers	$\mathfrak{B}$	Total number of RBs per OFDM symbol
Q	Number of subcarriers per RB	P_I	Precoding indicator
$\mathbb{C}$	Set of complex numbers		

Furthermore, a list of important abbreviations and symbols used throughout this paper are summarized in Tables 1 and 2, respectively.

II. SYSTEM MODEL AND FUNDAMENTALS

A. SYSTEM MODEL

This work considers a typical OFDM-based LSAS [30], [31]. To simplify the presentation, we initially consider a single MBS and later extend the model to a multi cell scenario. The considered MBS is equipped with M transmit antennas, and simultaneously serves K single-antenna UEs, where $M \gg K$. The symbol vector $\mathbf{d}^n = [d_1, d_2, \ldots d_K]^T$, d_k is the data symbol of the kth user selected uniformly from a particular constellation such as quadrature amplitude modulation (QAM), and the index n specifies the corresponding nth subcarrier that will be used to transmit the data vector $\mathbf{d}^n$. For linearly precoded LSAS, the vector $\mathbf{d}^n$ is multiplied by an $M \times K$ precoding matrix $\mathbf{\Lambda}^n$ to generate the precoded vector $\mathbf{v}^n$. That is,

$$\mathbf{v}^n = \mathbf{\Lambda}^n \mathbf{d}^n \tag{1}$$

where $\mathbf{v}^n \in \mathbb{C}^{M\times 1}$. To generate M OFDM symbols with N subcarriers each, the following matrix is formed,

$$\mathbf{V} = \begin{bmatrix} \mathbf{v}_1^T \\ \mathbf{v}_2^T \\ \vdots \\ \mathbf{v}_N^T \end{bmatrix} \tag{2}$$

where $\mathbf{V} \in \mathbb{C}^{N\times M}$. Consequently, each column in $\mathbf{V}$ is converted to an OFDM symbol by computing the inverse fast Fourier transform (IFFT) and appending a cyclic prefix (CP). Then each OFDM symbol is mapped to one of the M antennas.

At the receiving side, each UE removes the CP samples and computes the FFT of the received sequence to produce the vector $\mathbf{r}$, which contains the information symbols of the K users. At the nth subcarrier, $\mathbf{r}$ can be written as

$$\begin{aligned} \mathbf{r}^n &= \mathbf{H}^n \mathbf{v}^n + \mathbf{w}^n \\ &= \mathbf{H}^n \mathbf{\Lambda}^n \mathbf{d}^n + \mathbf{w}^n \end{aligned} \tag{3}$$

where $\mathbf{H}^n \in \mathbb{C}^{K\times M}$ is the channel matrix and $\mathbf{w}^n \in \mathbb{C}^{K\times 1}$ represents the receiver noise that has independent and identically distributed (i.i.d.) circularly symmetric complex Gaussian entries with zero-mean and σ_w^2 variance.

The K UEs require a set of different bit rates, $\bar{\mathbf{R}} \in \mathbb{R}^{1\times K}$, which are subject to certain latency requirements defined by $\bar{\mathbf{Y}} \in \mathbb{R}^{1\times K}$. In this paper, latency is defined as the data transmission duty cycle for a given UE. This is defined as the ratio between the required OFDM symbols and the number of transmission slots per frame.

A modified time-division duplex (TDD) system is considered with low density UE distribution, as in rural and suburban areas. The considered frame structure follows the format described in [36], where a frame consists of F OFDM data symbols and includes ℓ OFDM pilot symbols. Therefore, each frame has $F-\ell$ data symbols for uplink (UL) and downlink (DL) transmissions, denoted as F_{D} and F_{U}, respectively. In this work we consider that $F_{\mathrm{D}} = F_{\mathrm{U}}$ and $\ell = F/10$, where $F = T_{\mathrm{u}} T_{\mathrm{fr}} / \left(T_{\mathrm{g}} T_{\mathrm{s}}\right)$ [36], T_{g} is the OFDM cyclic prefix interval, T_{s} is the OFDM symbol interval, T_{fr} is the total frame period and T_{u} is the OFDM usable interval, $T_{\mathrm{u}} = T_{\mathrm{s}} - T_{\mathrm{g}}$. The pilot symbols are used to estimate the channel response using the MMSE criterion [37].

As proposed by the Greentouch consortium [7], we consider separate pilot and control signal transmission to allow each MBS to hibernate when there is no data or pilot signals to be transmitted. Furthermore, it is assumed that each MBS has the ability to control the number of active antennas, which can be activated/deactivated instantly. A reuse factor of 7 is assumed for the pilot signal transmission and the pilot

signals are orthogonal in the time domain. Therefore, the pilot length for the k^{th} UE is given by $\mathcal{K} \leq \ell_k \leq \ell/7$, where $\mathcal{K}$ is the maximum number of instantaneous multiplexed UEs. As reported in [36], this pattern reduces pilot contamination to a value that is much lower than the noise level, making it plausible to ignore the impact of pilot contamination. In the frequency domain, the subcarriers are divided into resource blocks (RBs) each of which has 12 subcarriers, and time-spectrum will be allocated for each RB and OFDM symbol.

B. SINR AND CAPACITY MODEL

For clarity, we first describe the signal-to-interference and noise ratio (SINR) and the capacity formulae of the precoding schemes used as the basis for the proposed algorithm. The precoding process can take a maximum of $\mathcal{K}$ UEs per RB where $\mathcal{K} \leq K$. Given that the average SNR at the kth UE for a single antenna system is given by [4],

$$\psi_k|\alpha_k = \frac{\alpha_k^{-1} P_D}{\eta_k} \tag{4}$$

where α_k is the pathloss coefficient between the MBS and kth UE, P_D is the transmit power per antenna at the MBS and η_k is the noise power of the UE. The effective SINR of the kth UE with M active antennas, $\mathcal{K}$ active UEs, with imperfect channel estimates, can be expressed as [4],

$$\gamma_k = \frac{M}{\mathcal{K}} a_k + \mu \tag{5}$$

where $\mu = 0$ and $-a_k$ for CJ and ZF precoding, respectively, and

$$a_k = \begin{cases} \dfrac{\psi_k \varrho_k}{(\psi_k + 1)(\varrho_k + 1)}, & \text{CJ precoding} \\ \dfrac{\psi_k \varrho_k}{\psi_k + \varrho_k + 1}, & \text{ZF precoding.} \end{cases} \tag{6}$$

Furthermore, $\varrho_k = \ell_k P_{\text{U}} / (\alpha_k \eta_0)$, where η_0 is the noise power at the MBS. Since a large number of antennas can eliminate small scale fading variations [3], the effective SINR for the precoded system is the same across all RBs. Given that each OFDM symbol has a maximum of $\mathfrak{B}$ RBs that can be allocated to a particular user, the maximum achievable bit rate for that user is given by,

$$R_k^{\max} = \frac{1}{T_{\text{fr}}} F \mathfrak{B} Q \log_2 (1 + \gamma_k) \quad \text{bit/s} \tag{7}$$

where Q is the number of subcarriers per RB. Based on (4)-(7), LSAS will have a set of pathloss coefficients, $\boldsymbol{\alpha} \in \mathbb{R}^{1\times K}$, received interference power set, $\bar{\mathbf{I}} \in \mathbb{R}^{1\times K}$, to calculate the SINR set $\boldsymbol{\gamma} \in \mathbb{R}^{1\times K}$ and the achievable bit rate $\bar{\mathbf{R}}^{\max} \in \mathbb{R}^{1\times K}$. To simplify notations, $\boldsymbol{\gamma}_G$, $\boldsymbol{a}_G$, $\boldsymbol{\mu}_G$ and $\bar{\mathbf{R}}_G^{\max}$ are used for CJ precoding and $\boldsymbol{\gamma}_Z$, $\boldsymbol{a}_Z$, $\boldsymbol{\mu}_Z$ and $\mathbf{R}_Z^{\max}$ for ZF precoding.

C. ENERGY EFFICIENCY MODEL

The EE computed over a given frame is computed in this work in terms of the energy productivity of the system, which is defined as

$$\begin{aligned} \mathcal{E} &= \frac{B_{\text{fr}}^{\Sigma}}{P^{\Sigma} T_{\text{fr}}} \text{ bits/Joule} \\ &= \frac{B_{\text{fr}}^{\Sigma} / T_{\text{fr}}}{P^{\Sigma}} \end{aligned} \tag{8}$$

where P^{Σ} is the total consumed power and B_{fr}^{Σ} is the total number of bits transmitted per frame. By noting that $B_{\text{fr}}^{\Sigma}/T_{\text{fr}}$ simply represents the total DL bit rate R^{Σ}, then

$$\begin{aligned} \mathcal{E} &= \frac{R^{\Sigma}}{P^{\Sigma}} \\ &= \frac{1}{P^{\Sigma}} \sum_{k=1}^{K} \min \left\{ R_k, R_k^{\max} \right\}. \end{aligned} \tag{9}$$

The data rate for each user is selected as $\min \left\{ R_k, R_k^{\max} \right\}$ to minimize the energy consumption. Therefore, the MBS will limit the total bit rate to the desired rate even when higher bit rates can be achieved.

The total power consumption P^{Σ} is related to the DL transmission model for the 2020 scenarios [7] is given by

$$P^{\Sigma} = P_A + P_B + P_C + P_H + P_J \tag{10}$$

where P_A denotes the power consumption of the power amplifier (PA), P_B is the digital baseband power, P_C is the antenna analog circuit power, P_H is the power for signaling and control bits, and P_J is the power consumption related to the control, backhaul and network signaling, which is typically 300m̃W [7], [38], [39]. The powers P_A, P_B and P_C are assumed to be adaptive where it switches between active (on) and hibernation (off) states, where at a given instant, M antennas are active for $\bar{\boldsymbol{\varepsilon}} \in \mathbb{R}^{1\times M}$ percent of the time slot. Hence, $P_A = \sum_{m=1}^{M} P_A^{\text{on}} \varepsilon_m + (1 - \varepsilon_m) P_A^{\text{off}}$, $P_B = \sum_{m=1}^{M} \varepsilon_m P_B^{\text{on}}$ and $P_C = \sum_{m=1}^{M} \varepsilon_m P_C^{\text{on}}$, where $P_A^{\text{on}} = \max \left\{ \frac{\varphi}{\nu_A} P_D, P_A^{\min} \right\}$, φ is the power coefficient, $P_A^{\min}$ is the minimum power consumption of the PA and is equal to 28.75 mW, ν_A is the PA efficiency, which is considered as 0.5, and $P_A^{\text{off}} = 4.375$m̃W. Furthermore, $P_C^{\text{off}} = 150$m̃W and $P_B^{\text{on}} = 16$m̃W.

The power for signaling and control bits is $P_H = \frac{E_H^{\text{ref}}}{3} \sum_{k=1}^{K} R_k$, where E_H^{ref} is the energy intensity of the signaling and control given in [7], which equals to 0.35 J/Mbits and 0.06 J/Mbits for suburban environments with 0.75 UEs per km^2 and 5.25 UEs per km^2, respectively, and 1.99 J/Mbits and 0.3 J/Mbits for rural environments with 0.075 UEs per km^2 and 0.525 UEs per km^2, respectively.

III. THE ADAPTIVE LSAS ALGORITHM

A. ALSAS DESIGN PRINCIPLE

ALSAS aims to satisfy the UEs' QoS requirements with the minimum transmit power by intelligently utilizing prior

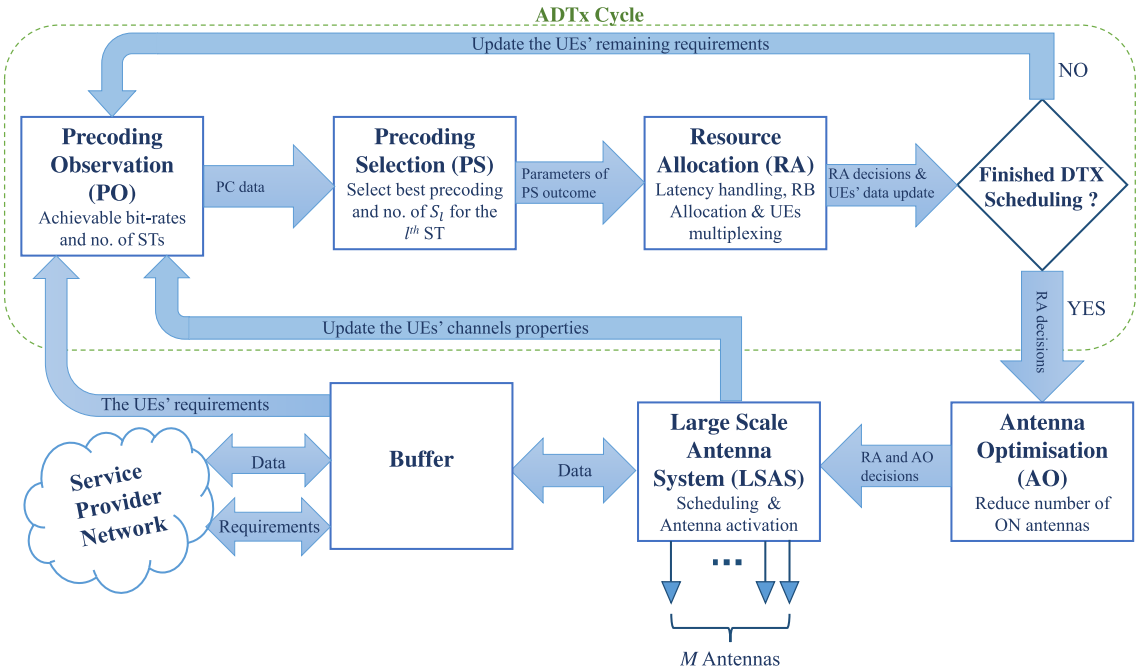

FIGURE 1. ALSAS design principle.

knowledge of the requirements to adapt various system parameters. The adaptation process can be performed in two main stages as shown in Fig. 1. In the first stage, the main LSAS subsystems, which are responsible for signal transmission/reception as well as the UEs' measurement, detect the main UEs' properties, such as pathloss, interference information, etc., and pass them to the ADTx stage to determine the transmission scheduling accordingly.

In the second stage, the ADTx reduces the transmission time based on the UEs bit rate and latency requirements through a *buffering* system. Such requirements are considered because the UEs support various types of applications with different data rate requirements. For example, VoIP requires low bit rates in a continuous fashion, but ultra high definition (UHD) video streaming requires high data rates that is at least 40 Mbps, but it can be bursty if the user is streaming short videos [40]. Therefore, AAO can be used to reduce the number of active antennas without compromising the achievable bit rate by adjusting the transmission period according to a predefined criterion.

B. THE ADTx STAGE

The ADTx stage arranges the data into L scheduled transmissions (STs), and determines the precoding technique that minimizes the total required transmission time for each ST, subject to a given complexity constraint. Each ST contains data for one or more UE to be transmitted simultaneously, thus, resource allocation in the form of RB assignment is performed. For each ST, the allocation process specifies the number of required OFDM symbols $\bar{\boldsymbol{\mathcal{S}}} \in \mathbb{I}^{1\times L}$, number of active antennas $\bar{\boldsymbol{\mathcal{M}}} \in \mathbb{I}^{1\times L}$, and the RB allocation matrix $\boldsymbol{\mathcal{A}} \in \mathbb{B}^{K\times\mathcal{N}}$. The elements of $\boldsymbol{\mathcal{A}}$ and $\bar{\boldsymbol{\mathcal{S}}}$ are affected by the UEs' requirements such as the data rates $\bar{\mathbf{R}}$ and latencies $\bar{\mathbf{Y}}$, and channel conditions including pathloss and time correlation.

The need for adaptive precoding can be justified by noting that CJ enables using all M antennas at the expense of significant multiple access interference. On the other hand, ZF eliminates the interference, but it limits the number of antennas that can be used due to the large delay associated with processing the precoding matrix [41]. In this paper, we assume that ZF can only use a subset of $M_Z < M$ antennas. The choice of which precoding technique is used at the lth ST is influenced by M_Z, the maximum number of multiplexed UEs when using CJ $\mathcal{K}_G$, or ZF $\mathcal{K}_Z$, as well as $\boldsymbol{\psi}$, $\bar{\boldsymbol{R}}$ and $\bar{\mathbf{L}}$, where $M_Z < M$ and $\mathcal{K}_G > \mathcal{K}_Z$. UEs that require transmission at the lth ST are indicated by the set $\boldsymbol{\xi} \in \mathbb{B}^{1\times K}$, where $\xi_k = 1$ indicates that the kth UE requires an ST, otherwise $\xi_k = 0$. The ADTx stage during the lth ST can be best described using the following steps:

1) Set $l = 1, \omega = 1$.
2) Compute PO.
3) Select the desired Precoding scheme.
4) Allocate Resources.
5) If $\sum_{k=1}^{K} R_{l,k} = 0$ *or* $S_{l+1} = 0$, end.
6) Else, $l = l + 1, L = l$, Go to step 2.

Steps 2, 3 and 4 are described below, and ω is a weighting factor defined in **Algorithm 3**.

1) COMPUTING PO

The PO block provides all the required information for the precoder selection and resource allocation, which includes

the SINR, number of RBs for each UE, achievable bit rate and required OFDM symbols. The achievable bit rate per OFDM symbol for CJ and ZF requires the SINRs of the CJ and ZF precoders at the lth ST for all users, which are given by $\boldsymbol{\gamma}_{G,l} = \left[\gamma_{G,l}^{(1)}, \gamma_{G,l}^{(2)}, \ldots, \gamma_{G,l}^{(\mathcal{K}_{G,l})}\right]$ and $\boldsymbol{\gamma}_{Z,l} = \left[\gamma_{Z,l}^{(1)}, \gamma_{Z,l}^{(2)}, \ldots, \gamma_{Z,l}^{(\mathcal{K}_{Z,l})}\right]$, respectively, where

$$\gamma_{G,l}^{(k)} = \gamma_k|\left[M, \mathcal{K}_{G,l}, a_{G,k}, \mu_G\right], \quad k = 1, \ldots, \mathcal{K}_{G,l} \tag{11}$$
$$\gamma_{Z,l}^{(k)} = \gamma_k|\left[M_Z, \mathcal{K}_{Z,l}, a_{Z,k}, \mu_Z\right], \quad k = 1, \ldots, \mathcal{K}_{Z,l} \tag{12}$$

and $\mathcal{K}_{G,l}$ and $\mathcal{K}_{Z,l}$ are the number of multiplexed UEs at the lth ST,

$$\mathcal{K}_{G,l} = \min\{\mathcal{K}_G, K_l\}$$

and

$$\mathcal{K}_{Z,l} = \min\{\mathcal{K}_Z, K_l\}$$

K_l is the total number of users whose data will be transmitted during the lth ST, $\sum_{l=1}^{L} K_l = K$. Furthermore, the number of allocated RBs for the kth user during the lth ST using CJ precoding is given by

$$\mathcal{N}_{G,k,l} = \left\lfloor \frac{\mathcal{K}_{G,l}}{K_l}\mathfrak{B} \right\rfloor \xi_k, \quad k = 1, 2, \ldots, K_l \tag{13}$$

subject to:

$$\sum_{k=1}^{K_l} \mathcal{N}_{G,k,l} = \mathcal{K}_{G,l}\mathfrak{B} \tag{14a}$$
$$\mathcal{N}_{G,k} \leq \left\lfloor \frac{\mathcal{K}_{G,l}}{K_l}\mathfrak{B} \right\rfloor + 1. \tag{14b}$$

Similarly, the number of RBs using ZF precoding is given by

$$\mathcal{N}_{Z,k} = \left\lfloor \frac{\mathcal{K}_{Z,l}}{K_l}\mathfrak{B} \right\rfloor \xi_k \tag{15}$$

subject to:

$$\sum_{k=1}^{K} \mathcal{N}_{Z,k} = \mathcal{K}_{Z,l}\mathfrak{B} \tag{16a}$$
$$\mathcal{N}_{Z,k} \leq \left\lfloor \frac{\mathcal{K}_{Z,l}}{K_l}\mathfrak{B} \right\rfloor + 1. \tag{16b}$$

Finally, using $\mathcal{N}_{G,k}$ and $\mathcal{N}_{Z,k}$, the calculated bit rate per OFDM symbol for $k = 1, \ldots, K$ using CJ and ZF are given by

$$R_{G,k}^{\max} = R_G^{\max}\left(\gamma_{G,k,l}, \mathcal{N}_{G,k}\right) \tag{17}$$
$$R_{Z,k}^{\max} = R_Z^{\max}\left(\gamma_{Z,k,l}, \mathcal{N}_{Z,k}\right). \tag{18}$$

2) PRECODING SELECTION

In general, precoding selection leads to two possible outcomes, which are reducing the release time (RT) or increasing the spectral efficiency (SE). RT is defined as the time period taken for at least one UE to satisfy their bit rate requirement. Reducing RT benefits some UEs that significantly gain from a certain precoding choice, which in turn reduces the number of simultaneous UEs for the rest of the STs. However, this strategy may lead to blocking out the resource for the remaining UEs, especially at the cell edge. In order to overcome such a conflict, we propose the following:

- Precoding selection is based on minimizing the UEs' outage probability.
- Trade-off between minimizing RT and maximizing SE where these two parameters are selected alternately only in the case when the RT of CJ and ZF are similar. If, however, RT for one of the precoding schemes is much smaller than the other, the precoding technique that minimizes RT is selected.

RT of CJ and ZF at the l^{th} ST, is $s_G = \min_o\left(R_{l,o}/R_{G,o}^{\max}\right)$ and $s_Z = \min_o\left(R_{l,o}/R_{Z,o}^{\max}\right)$, respectively, where $o = \{k \mid k = 1, \ldots, K \wedge \xi_k = 1\}$, and $\wedge$ denotes the logical conjunction. In addition, the user that provides the minimum RT at the l^{th} ST is given by $u_{\min} = \arg\min_o \boldsymbol{\psi}_o$. Hence we can define RT from CJ and ZF at the l^{th} ST $\boldsymbol{\upsilon} = (s_G, s_Z)$ with its minimum and maximum values $\upsilon_{\min} = \min \boldsymbol{\upsilon}$ and $\upsilon_{\max} = \max \boldsymbol{\upsilon}$, respectively.

Minimizing RT takes the precoding technique that has the smallest value from set $\boldsymbol{\upsilon}$. Let the RT based precoding selection be denoted by $P_I \in \{0, 1\}$, where P_I is the precoding indicator, $P_I = 1$ implies that ZF is used and $P_I = 0$ means that CJ is used. Thus, the precoding selection can be given by

$$P_I = (\arg\min\{s_G, s_Z\}) - 1. \tag{19}$$

By noting that $\arg\min\{s_G, s_Z\} \in \{1, 2\}$, then $P_I \in \{0, 1\}$. On the other hand, SE based precoding selection compares the bit rates of the precoding techniques to select the one with the largest value. If the outcome of SE based precoding selection is given by $\Omega \in \{0, 1\}$, where $\Omega = 1$ corresponds to ZF and $\Omega = 0$ corresponds to CJ, then SE based precoding selection can be given by

$$\Omega = \mathrm{U}\left(\sum_{k=1}^{K} R_{G,k}^{\max}, \sum_{k=1}^{K} R_{Z,k}^{\max}\right). \tag{20}$$

Based on the aforementioned two objectives, **Algorithm 1** is devised to select the precoding scheme. This algorithm includes three main checks that are sequenced according to their priority. The first check is for the outage, which would arise if RT is longer than the available OFDM symbols at the l^{th} ST, S_l, and selects the precoding technique that minimizes the outage, which will be performed using **Algorithm 2**. However, if the two precoding techniques have identical outages, the algorithm performs the second check and selects the

precoding technique that offers the minimum RT. Otherwise, the algorithm proceeds to check three and selects the precoding technique that maximizes SE, which will be performed using **Algorithm 3**. It is worth noting that **Algorithm 3** guarantees that RT minimization is still considered when the overall outage probability for the users is minimized. This is achieved by using a weighting factor $\omega \in \{1, 2\}$, as shown in **Algorithm 3**.

The outcome of precoding selection at the l^{th} ST will be defined as

$$\mathcal{P}_l = \begin{cases} 1, & \text{ZF is selected} \\ 0, & \text{CJ is selected.} \end{cases} \tag{21}$$

Using the selected precoding technique, the global parameters for the l^{th} ST, are given by $\mathcal{M}_l = M$, $\mathcal{K}_l = \mathcal{K}_{G,l}$, $a_l = a_G$, $\mu_l = \mu_G$ and $\mathcal{N}_l = \mathcal{N}_G$ if $\mathcal{P}_l = 0$; otherwise, $\mathcal{M}_l = M_Z, \mathcal{K}_l = \mathcal{K}_{Z,l}, a_l = a_Z, \mu_l = \mu_Z$ and $\mathcal{N}_l = \mathcal{N}_Z$.

Algorithm 1 Precoding Selection

Input: $\mathbf{R}$, $\mathbf{R}_Z^{\max}$, $\mathbf{R}_G^{\max}$, s_G, s_Z, S_l, $\boldsymbol{\upsilon}$

1. **if** $s_G > S_l$ **OR** $s_Z > S_l$
2. Perform **Algorithm 2**
3. **elseif** $\upsilon_{\min} < 2\upsilon_{\max}$ **OR** $\omega = 2$, **then**
4. $\mathcal{P}_l = P_I$, $\mathcal{S}_l = \upsilon_{\min}$, $\omega = 1$
5. **else**
6. Perform **Algorithm 3**
7. **end**
8. Output: $\mathcal{S}_l$, $\mathcal{P}_l$, ω

Algorithm 2 Outage Users Based Precoding Selection

Input: $\boldsymbol{R}$, $\mathbf{R}_G^{\max}$, $\mathbf{R}_Z^{\max}$, $\mathbf{R}_l$, $\boldsymbol{\upsilon}$, S_l

1. $\mathfrak{X}_Z = \sum_i \mathrm{U}\left(R_i, R_{l,i} - R_{Z,i}^{\max}\right)$
2. $\mathfrak{X}_G = \sum_i \mathrm{U}\left(R_i, R_{l,i} - R_{G,i}^{\max}\right)$
3. **if** $\mathfrak{X}_Z \neq \mathfrak{X}_G$, **then** $\mathcal{P}_l = \mathrm{U}(\mathfrak{X}_Z, \mathfrak{X}_G)$
4. **else,** $\mathcal{P}_l = \left\{\left(\sum_{k=1}^{K} R_{Z,k}^{\max}\right) > \left(\sum_{k=1}^{K} R_{G,k}^{\max}\right)\right\}$
5. **end if**
6. $\mathcal{S}_l = \begin{cases} S_l, & S_l < 0.1 \text{ OR } (\mathfrak{X}_Z = 0 \text{ AND } \mathfrak{X}_G = 0) \\ \frac{1}{2}S_l, & \text{otherwise} \end{cases}$
7. **Output:** $\mathcal{P}_l$, $\mathcal{S}_l$

3) RESOURCE ALLOCATION

The final aspect in the ADTx stage is to utilize the information gathered to perform resource allocation which takes into account latency handling. After completing the precoding selection, resource re-allocation is needed if the latency constraints are not satisfied. A possible approach to overcome this is to increase the transmission time such that the latency constraint can be satisfied. However, this may reduce the system efficiency because it introduces transmission redundancy. Therefore, we propose **Algorithm 4** to maintain redundancy within a pre-defined limit. Recalculating the number of RBs for the l^{th} ST is given by $\widehat{\boldsymbol{\mathcal{N}}}_l$ subject to $\min \sum_{k=1}^{K} \left| R_{l,k} - \hat{R}_k^{\max} \right|$ and $\min \sum_{k=1}^{K} \left| \sum_{b=1}^{l} \mathcal{S}_b \xi_k - Y_k \right|$. In order to minimize the complexity of the proposed scheme, the maximum number of iterations is set to three, which is selected on the basis that the impact of resource re-allocation becomes negligible beyond three iterations.

Algorithm 3 SE Based Precoder Selection

Input: $\mathbf{R}_G^{\max}$, $\mathbf{R}_Z^{\max}$, $\boldsymbol{\upsilon}$, Ω

1. $\lambda_Z = \sum_{i=1} \mathrm{U}\left(R_{G,i}^{\max}, R_{Z,i}^{\max}\right)$
2. $\lambda_G = \sum_{i=1} \mathrm{U}\left(R_{Z,i}^{\max}, R_{G,i}^{\max}\right)$
3. **if** $\lambda_Z \neq \lambda_G$, **then** $\mathcal{P}_l = \mathrm{U}(\lambda_G, \lambda_Z)$
4. **else**, $\mathcal{P}_l = \Omega$
5. **end if**
6. **if** $P_I \neq \mathcal{P}_l$, **then** $\omega = 2$, $\mathcal{S}_l = \max\left\{\frac{\upsilon_{\mathcal{P}_l+1}}{\omega}, \upsilon_{P_I+1}\right\}$
7. **else,** $\omega = 1$, $\mathcal{S}_l = \upsilon_{P_I+1}$
8. **end if**
9. **Output:** $\mathcal{P}_l$, $\mathcal{S}_l$, ω

Based on $\boldsymbol{\mathcal{N}}_l$, UEs multiplexing and RBs allocation is given by

$$\mathcal{A}_{l,k,n} = \begin{cases} 1, & \text{allocate } k^{\text{th}} \text{ UE at the } n^{\text{th}} \text{ RB} \\ 0, & \text{otherwise} \end{cases} \tag{22}$$

subject to:

$$\sum_{n=1}^{\mathfrak{B}} \mathcal{A}_{l,k,n} = \mathcal{N}_{l,k} \tag{23a}$$

$$\mathcal{A}_{l,n}^{\Sigma} \leq \mathcal{K}_l, \quad n = 1, \ldots, \mathfrak{B} \tag{23b}$$

where $\bar{\boldsymbol{\mathcal{A}}}^{\Sigma} \in \mathbb{R}^{1 \times \mathfrak{B}}$, and $\mathcal{A}_{l,n}^{\Sigma} = \sum_{k=1}^{K} \mathcal{A}_{l,k,n}$, $n = 1, \ldots, \mathfrak{B}$. Using $\mathcal{S}_l$ and R_l, the available symbols and remaining bit rates for the $(l+1)^{\text{th}}$ ST are respectively given by $S_{l+1} = F_{\mathrm{D}} - \sum_{b=1}^{l} \mathcal{S}_b$ and $R_{l+1,k} = R_k - \sum_{b=1}^{l} R_{b,k}^{\max} \mathcal{S}_b$, $k = 1, \ldots, K | \xi_k = 1$.

Algorithm 4 Latency Handling

Input: $\boldsymbol{\mathcal{N}}_l$, $\mathbf{R}^{\max}$, $R_{\text{target},k}$, $\mathbf{Y}$

1. $\mathrm{i} = 1$
2. **while** $\mathrm{i} \leq 3$ **do**
3. Adjust the number of RBs, $\widehat{\boldsymbol{\mathcal{N}}}_l$, based on the target, $R_{\text{target},l,k}$
4. Check the achievable bit rate, $\hat{\mathbf{R}}^{\max}$, using $\widehat{\boldsymbol{\mathcal{N}}}_l$ set
5. **If** $\hat{R}_k^{\max} > R_{\text{target},k}$ for any $k = 1, \ldots, K$ **then**
6. $\mathrm{i} = \mathrm{i}+1$, reduce number of multiplexed UEs, $\mathcal{K}_l$ and repeat line 3
7. **else**, $\mathrm{i} = 4$, $\mathcal{N}_{l,k} = \widehat{\mathcal{N}}_{l,k}$ for $k = 1, \ldots, K$
8. **end if**
9. **Output:** $\boldsymbol{\mathcal{N}}_l$, $\boldsymbol{\mathcal{S}}_l$, and $\mathcal{K}_l$

C. ANTENNA ARRAY OPTIMIZATION STAGE

The AAO stage attempts to reduce the number of active antennas required for each ST by adjusting the transmission period

based on $R = S\log_2\left(1+M\frac{a}{\mathcal{K}}\right)$. For example, assuming $\frac{a}{\mathcal{K}} = 1$ and $M = 400$, increasing the transmission time by 30% allows reducing the number of required antennas by 75%, and hence, provide further power saving. If the required number of antennas for the l^{th} ST after the AAO is denoted as $\tilde{\mathcal{M}}_l$, the AAO attempts to find min $\tilde{\mathcal{M}}_l$ subject to

$$\sum_{l=1}^{L}\tilde{\mathcal{S}}_l \le \mathcal{T}_{\text{D}} \tag{24a}$$

$$\tilde{R}_{l,k}^{\max}\mathcal{S}_l \le \lambda_{l,k},\ k=1,\ldots,K \tag{24b}$$

$$2\mathcal{K}_l \le \tilde{\mathcal{M}}_l \le M \tag{24c}$$

where $\tilde{\mathcal{S}}_l$ is the number of OFDM symbols at the l^{th} ST and $\tilde{R}_{l,k}$ is the bit rate for the kth UE during the l^{th} ST after the AAO step. $\tilde{R}_{l,k}$, $k = 1,\ldots,K$, is given by $\tilde{R}_{l,k} = \tilde{\mathcal{S}}_l\mathcal{C}\left(\gamma\left(\tilde{\mathcal{M}}_l,\mathcal{K}_l,a_{l,k},\mu_{l,k}\right),\mathcal{N}\right)$, where

$$\mathcal{C}\left(\gamma\left(\cdot\right),\mathcal{N}\right) = \frac{\mathcal{N}Q}{T_{\text{fr}}}\log_2\left(1+\gamma\left(\cdot\right)\right). \tag{25}$$

IV. ADTx ANALYSIS

A. SINR ANALYSIS OF THE DTX TRANSMISSION

1) SINGLE CELL LSAS WITH K UES UNIFORMLY PLACED WITHIN A DISTANCE $d_{\max}$

This scenario considers the case when the interference impact of LSAS to the surrounding cells is low. We assume that the pathloss is given by $\alpha = 10^{(\alpha_{\text{dB}}/10)}$, where $\alpha_{\text{dB}} = A + B\log_{10}(d)$, A is a constant that captures the effect of free space propagation at a reference distance d, and $B = 10\beta$, where β is the pathloss exponent. In the following analysis, the UE index is dropped, unless it is necessary to include it.

Lemma 1: The probability and cumulative density functions (PDF) and (CDF) of the UE's SINR are respectively given by

$$f_\psi\left(\psi\right) = \begin{cases} \dfrac{20}{\psi B d_{\max}^2}\left(\dfrac{\varpi}{\psi}\right)^{\frac{20}{B}}, & \psi \ge \psi_{\min} \\ 0, & \text{otherwise} \end{cases} \tag{26}$$

$$F_\psi\left(\psi\right) = \begin{cases} \dfrac{1}{d_{\max}^2}\left(\left(\dfrac{\varpi}{\psi_{\min}}\right)^{\frac{20}{B}} - \left(\dfrac{\varpi}{\psi}\right)^{\frac{20}{B}}\right), & \psi \ge \psi_{\min} \\ 0, & \text{Otherwise.} \end{cases} \tag{27}$$

where $\varpi = P_T/\left(\eta 10^{A/10}\right)$, η is the noise level at the UE, and the SINR per antenna $\psi = P_T/(\alpha\eta)$. The proof is given in Appendix II.

2) K UEs TRANSMITTING USING L STs

Consider the case where K UEs are transmitting over L STs, and each ST consists of K_l UEs, $\sum_{l=1}^{L}K_l = K$. The UEs are grouped based on their SINR values in ascending order, e.g. the UE with the lowest SINR is transmitted during the first ST, and the one with the highest SINR is transmitted in the L^{th} ST. The UE whose SINR order is m during the mth ST is denoted as u_m.

Lemma 2: The PDF of the SINR of the u_m^{th} UE is given by

$$f_{u_m}\left(\psi\right) = \frac{Kb}{r}\binom{K-1}{u_m-1}\sum_{t=0}^{\phi_m}\binom{\phi_m}{t}q^t \times\left(g\psi^{\frac{1}{rh_m}(h_m+t-\lambda)} - \psi^{\frac{1}{rh_m}(t-\lambda)}\right)^{h_m} \tag{28}$$

where $\phi_m = K-u_m$, $b = \varpi^{\frac{20}{B}}/d_{\max}^2$, $v = \frac{1}{d_{\max}^2}\left(\frac{\varpi}{\psi_{\min}}\right)^{\frac{20}{B}}$, $q = \frac{1-v}{b}$, $h_m = u_m - 1$, $r = \frac{B}{20}$, $\lambda = r+K$, and $g = v/b$.

Proof: Using order statistics, the SINR PDF of u_m^{th} UE is given by [42]

$$f_{u_m}\left(\psi\right) = W_m f_\psi\left(\psi\right)\left(F_\psi\left(\psi\right)\right)^{u_m-1}\left(1-F_\psi\left(\psi\right)\right)^{K-u_m}. \tag{29}$$

where $W_m \triangleq K\binom{K-1}{u_m-1}$. Expanding (29) gives

$$f_{u_m}\left(\psi\right) = \frac{W_m}{rd_{\max}^2\psi}\left(\frac{\varpi}{\psi}\right)^{\frac{1}{r}}\left(v-\sigma\left(\frac{\varpi}{\psi}\right)^{\frac{1}{r}}\right)^{u_m-1} \times\left(1-v+\sigma\left(\frac{\varpi}{\psi}\right)^{\frac{1}{r}}\right)^{K-u_m} \tag{30}$$

where $\sigma = 1/d_{\max}^2$. After some straightforward manipulations (30) can be written as

$$f_{u_m}\left(\psi\right) = \frac{\Lambda_l}{\psi^{\frac{20}{B}+1}}\left(v-\frac{b}{\psi^{\frac{20}{B}}}\right)^{u_m-1}\left(1-v+\frac{b}{\psi^{\frac{20}{B}}}\right)^{K-u_m} \tag{31}$$

where

$$\Lambda_m = \frac{Kb}{r}\binom{K-1}{u_m-1}. \tag{32}$$

By defining $\psi^{\frac{20}{B}} \triangleq x$, and noting that $b > 0$, $\{\phi_m,u_m\}$ are integers greater than one, thus $f_{u_m}\left(\psi\right)$ can be written as

$$f_{u_m}\left(x^{\frac{B}{20}}\right) = \frac{\Lambda_m}{x^{r+1}}\left(\frac{v}{b}-\frac{1}{x}\right)^{u_m-1}\left(\frac{1-v}{b}+\frac{1}{x}\right)^{\phi_m} \tag{33}$$

which can be further simplified to

$$f_{u_m}\left(x^{\frac{B}{20}}\right) = \frac{\Lambda_m}{x^{\lambda}}\left(gx-1\right)^{h_m}\left(qx+1\right)^{\phi_m}. \tag{34}$$

Using binomial expansion and substituting x with $\psi^{\frac{20}{B}}$ gives the PDF of u_m^{th}-ranked UE given in (28). □

B. TRANSMISSION PERIOD OF ADTx

Under scenario 2 and assuming that all UEs require the same throughput, R, the transmission length of the l^{th} ST is affected by the lowest SINR for that particular group. This implies that

$$S_l = \max_{u_m=1,\ldots,K_l}\frac{R}{C_l} \tag{35}$$

TABLE 3. Simulation parameters for Fig. 2 and 3, [7].

Parameter	Suburban	Rural
A	139.1	136.6
β	3.76	3.86
$d_{\min}$ (m)	35	35
$d_{\max}$(km)	1	1.345
T_{fr} (ms)	45	45
$\mathfrak{B}$	100	100

where

$$\mathcal{C}_l = \begin{cases} \dfrac{Q}{T_{\text{fr}}} \log_2 \left(1 + \dfrac{M}{K_l} \dfrac{\psi_{l,u_m}}{(\psi_{l,u_m}+1)}\right), & \text{CJ} \\ \dfrac{Q}{T_{\text{fr}}} \log_2 \left(1 + \dfrac{M_Z - K_l}{K_l} \psi_{l,u_m}\right), & \text{ZF.} \end{cases} \tag{36}$$

Hence, the average transmission period for scenario 2 is given by $\overline{S} = \sum_{l=1}^{L} \overline{S}_l$, where

$$\overline{S}_l = \int_{-\infty}^{\infty} f_{u_m}(\psi)\, S_l(\psi) d\psi \tag{37}$$

where

$$S_l(\psi) = \begin{cases} \dfrac{RT_{\text{fr}}}{Q} \left[\log_2 \left(1 + \dfrac{M}{K_l} \dfrac{\psi_{l,u_m}}{(\psi_{l,u_m}+1)}\right)\right]^{-1}, & \text{CJ} \\ \dfrac{RT_{\text{fr}}}{Q} \left[\log_2 \left(1 + \dfrac{M_Z - K_l}{K_l} \psi_{l,u_m}\right)\right]^{-1}, & \text{ZF.} \end{cases} \tag{38}$$

Assuming that in each ST, adaptive precoding selection is applied based on the following condition:

$$\mathcal{P}_l = \begin{cases} 1, & \psi_{l,u} \geq \psi_Z \\ 0, & \psi_{l,u} < \psi_Z \end{cases} \tag{39}$$

where $\psi_Z = M/(M_Z - K_l) - 1$, then, (37) can be written as

$$\overline{S}_l = \int_{\psi_{\min}}^{\psi_Z} f_{u_m}(\psi)\, S_l(\psi) d\psi + \int_{\psi_Z}^{\psi_{\max}} f_{u_m}(\psi)\, S_l(\psi) d\psi. \tag{40}$$

Since $1/\log(x/(x+1))$ does not have a definite integral, the solution of this equation is achieved numerically.

V. NUMERICAL RESULTS

A. IMPACT OF ADTx

The impact of discontinuous transmission on LSAS is evaluated in Figs 2 and 3 for the suburban and rural scenarios, respectively. LSAS is considered to have $M = 400$ antennas, where each antenna transmits 200 mW of power. The simulation parameters are given in Table 3. The channel attenuation factors include the building penetration [7], [43]. The analytical results are obtained using (40).

As can be noted from Figs 2 and 3, the analysis and simulation results match almost perfectly, which confirms the validity of the derived analysis. As can be seen from these figures, increasing the number of STs reduces the total number of occupied slots. The optimum number of STs vary depending on the number of active UEs. For example, the minimum number of transmission slots for $K = 5$ and $K = 9$ is achieved using 2 and 3 STs, respectively. This shows that the proposed ADTx can reduce the required transmission period and allows switching off some of the LSAS components.

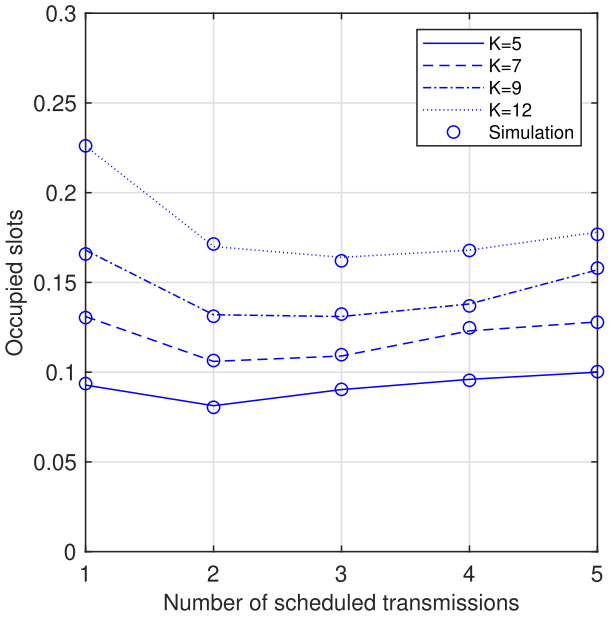

FIGURE 2. Impact of various number of scheduled transmission in suburban scenario.

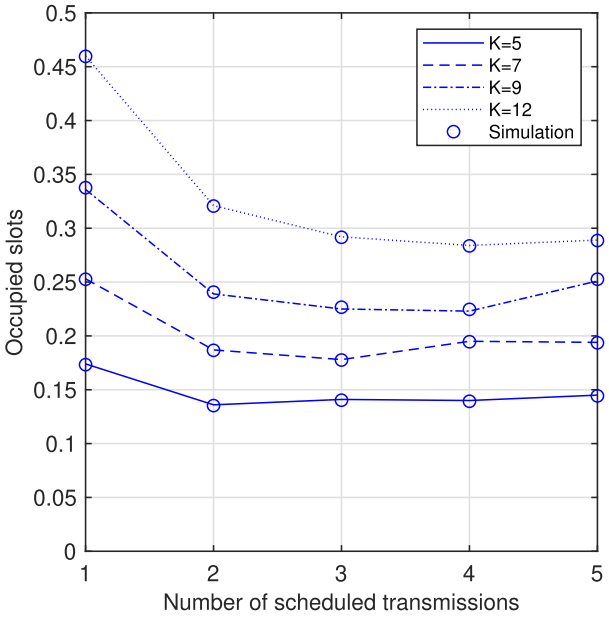

FIGURE 3. Impact of various number of scheduled transmission in rural scenario.

B. EVALUATION PARAMETERS FOR MULTI CELL SCENARIOS

The performance evaluation considered in this subsection focuses on EE and the outage probability performance. The UEs outage represents the number of UEs that do not get

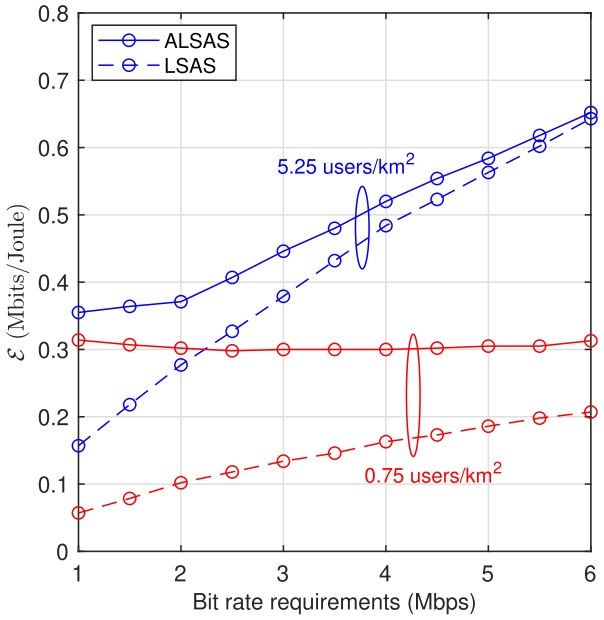

FIGURE 4. Energy productivity of suburban scenario with fixed rate requirement.

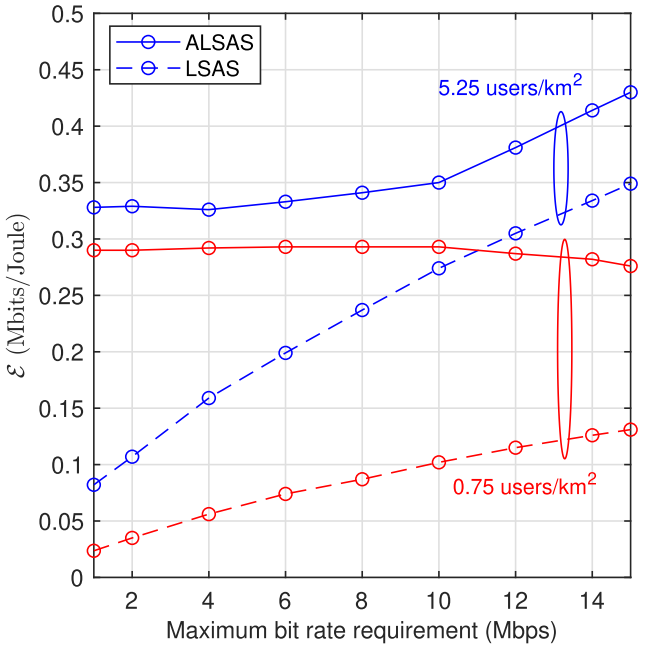

FIGURE 5. Energy productivity of suburban scenario with varying bit rate requirement.

at least half of the required bit rate. The presented results correspond to suburban and rural scenarios, which make up most of the coverage area of a cellular network, and hence, the EE improvement is expected to be significant. A typical users' density in suburban areas ranges between 0.75 and 5.25 UE per km^2, with a short inter-site-distances (ISD) of 1732.1 m. In rural areas, the users' density ranges between 0.075 and 0.525 UE per km^2 with ISD of 2330 m [9].

A 49 cell wrap around is considered [36], the carrier frequency is 2 GHz, and the pathloss is given by $\alpha_k = 10^{\frac{A+\mathcal{X}}{10}}(d_k)^{\frac{B}{10}}$ where $\mathcal{X}$ is log normal shadowing with zero mean and 6 dB standard deviation. The small scale fading is modeled as Rayleigh, and the noise floor at the MBS and UEs is set to -172 dBm/Hz and -165 dBm/Hz, respectively. Various cases of bit rate requirements are evaluated, which includes fixed and varying bit rate requirements. In the case of fixed bit rate requirements, the target bit rate is set to be in the range of 1 to 6 Mbps. On the other hand, in the case of varying bit rate requirements we assume a minimum bit rate of 100 kbps with the maximum bit rate between 1 to 15 Mbps. The bit rate is generated in a uniform distribution in logarithmic scale. For both cases, latency requirements between 10^{-3} and 5 duty cycles per frame is considered. The performance of the proposed scheme is compared to the continuous transmission case described in Appendix A.

The performance of the proposed ALSAS in a suburban scenario shown in Figs. 4, 5, and 6, where Fig. 4 and Fig. 5 considers the EE with fixed and variable bit rate requirements, while 6 presents the outage probability. As can be noted from Fig. 4, the proposed technique provides 125% EE improvement for a fixed bit rate requirement of 1 Mbps for the 5.25 users/km^2 case. When the user density decreases to 0.75 users/km^2, the EE improves substantially to 455%. As the bit rate requirement and number of UEs increase, the improvement decreases and becomes about 1% for the high density case, while it remains significant for the low density case with an improvement of about 52%. The EE improvement reduction at high data rate and user density is due to the fact that the MBS is mostly required to transmit over the entire transmission frame.

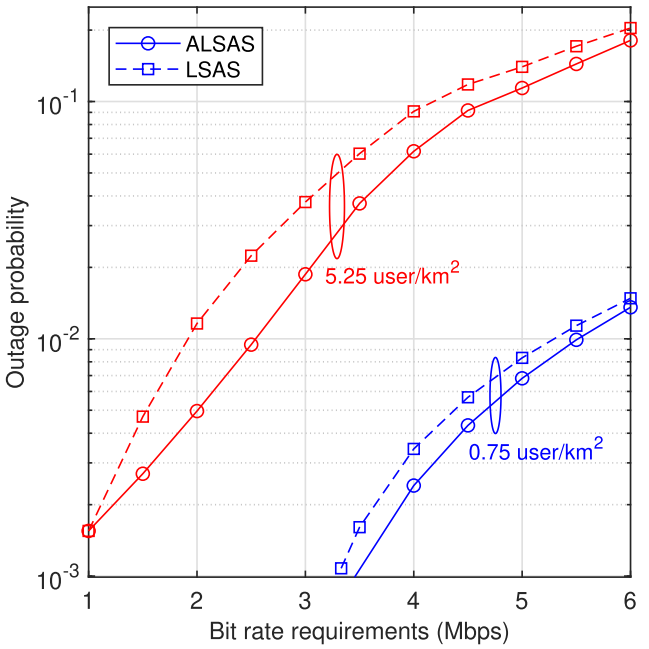

FIGURE 6. Outage probability of suburban scenario with fixed rate requirement.

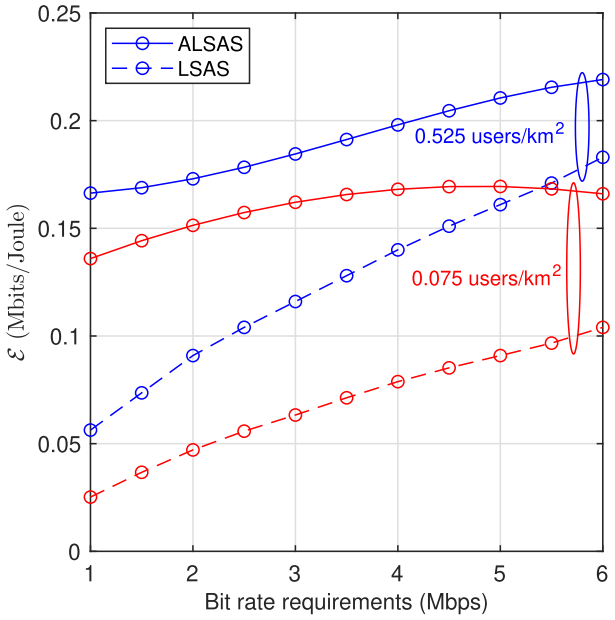

FIGURE 7. Energy productivity of rural scenario with fixed bit rate requirement.

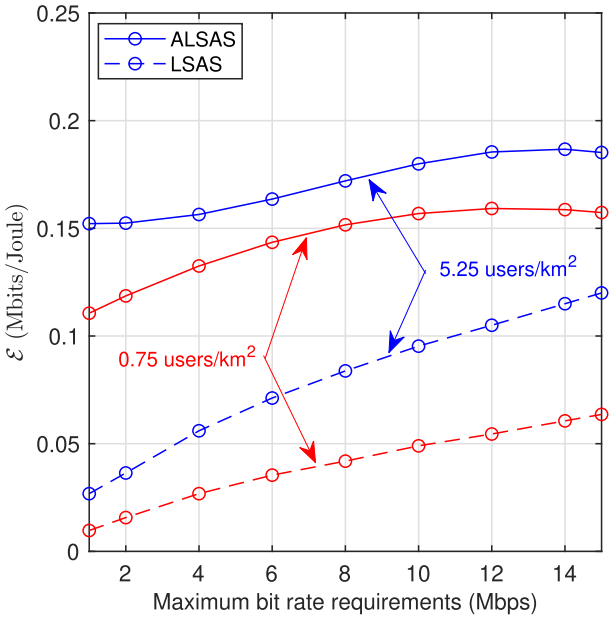

FIGURE 8. Energy productivity of rural scenario with varying bit rate requirement.

The EE for varying bit rate is shown in Fig. 5. As can be noted, the EE trends with variable bit rates are generally similar to the EE with fixed bit rates given in Fig. 4, except that the improvement is considerably higher, particularly for the low user density case. As can be noted from the figure, the proposed ALSAS, for the case of 0.75 UEs per km^2, provides improvement of 1124% and 118% for the maximum bit rate of 1 and 15 Mbps, respectively. For the high user density case, the EE improvement is 304% and 23% for 1 and 15 Mbps, respectively. Considering that most of the wireless mobile applications require bit rates less than 1.5 Mbps, the proposed technique will provide an energy saving of more than 1000% in this suburban scenario.

Fig. 6 shows the outage probability of the conventional and proposed adaptive LSAS techniques using fixed bit rate requirements. As the figure shows, ALSAS offers lower or equivalent outage probability for the considered bit rate range. Consequently, the EE improvement obtained using the ALSAS is achieved without compromising the outage probability.

Similar to the suburban scenario, the performance of the proposed ALSAS is depicted in Figs 7-10. The results are presented for fixed and variable bit rates and ISDs. The fixed ISD is used to evaluate the performance of the proposed technique with conventional configuration, while the varying ISD is used to evaluate the EE performance if the cellular operators of LSAS have ISD values that are from the one discussed in this paper. To evaluate the impact for various ISDs, the required fixed bit rate is set to 4 Mbps, and the varying bit rate ranges from 100 kbps to 10 Mbps. In both cases, the user density is considered as 0.525 UE/km^2.

Fig. 7 shows the EE for fixed ISD and fixed bit rates. Similar to the suburban scenario, the proposed technique improves the EE of the cellular network in rural scenarios without degrading the QoS. Fig. 7 shows that an EE improvement of more than 21% is guaranteed given that the bit rate requirement is less than 6 Mbps for all UEs. As can be seen from this figure, the proposed ALSAS provides a 61% EE for low loads such as 0.075 UE/km^2, even if the bit rate is 6 Mbps. When the load increases to 0.525 UE/km^2, the EE improvement surges to 196%.

Fig. 8 shows the EE for a fixed ISD and variable bit rates. As can be noted from this figure, the EE improvement for ALSAS at 0.075 UEs/km^2 is about 952% and 150% for a maximum bit rate of 1 and 15 Mbps, respectively. For the case of 0.525 UEs/km^2, the EE improvement is about 461% and 32% compared to conventional LSAS for a maximum bit rate of 1 and 15 Mbps, respectively. Considering that most applications require less than the simulated bit rate requirement, it can be concluded that a minimum of 150% EE improvement will be provided for future cellular networks.

The QoS in terms of outage probability is shown in Fig. 9 for the fixed rate and fixed ISD scenario. As depicted in this figure, the proposed ALSAS managed to offer an outage probability that is comparable to the one offered by the conventional LSAS for both low and high user densities.

The EE and outage probability for fixed and variable bit rates and ISDs are presented in Fig. 10 and Table 4, respectively. As can be noted form Fig. 10 and Table 4, conventional LSAS achieves a maximum EE at 2.6 and 3 km, while the proposed ALSAS improves EE as the ISD is reduced, without compromising the QoS. Such performance is obtained because reducing ISD decreases the total number of users and the overall pathloss between MBS and UEs. Consequently, the required transmission time and number of active antennas can be reduced. This further proves the capability of

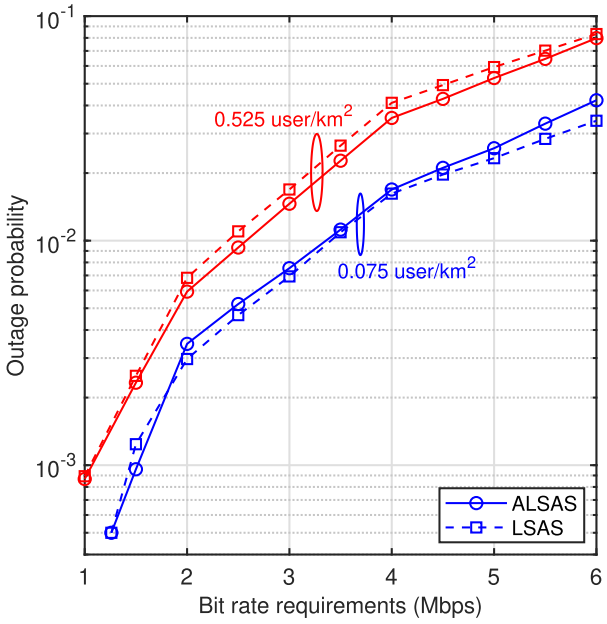

FIGURE 9. Outage probability of rural scenario with fixed rate requirement.

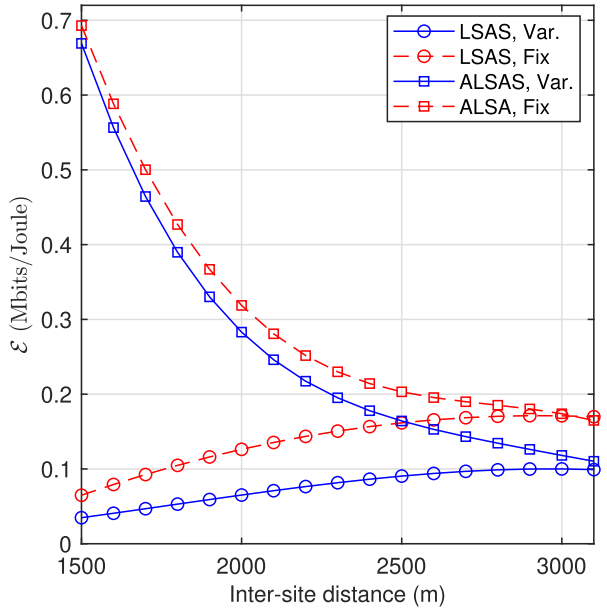

FIGURE 10. Energy Productivity performance of rural scenario at various distances.

the proposed technique to maximize the hibernation time of the MBS. The figure also shows that conventional transmission does not provide a significant EE improvement as ISD is varied. In practical scenarios, the bit rate requirement for certain UEs might be varying, thus, the proposed technique can provide up to 500% EE improvement over conventional LSAS. Although reducing ISD causes higher capital expenditure (CAPEX) for the cellular operator, it lowers the carbon footprint significantly, as well as improves the network performance due to shortening the distance.

TABLE 4. Outage probability of rural scenario at various distances.

ISD (km)	Fixed Rate		Variable Rate	
	ALSAS	LSAS	ALSAS	LSAS
1.9	9.7×10^{-4}	3.0×10^{-3}	1.3×10^{-3}	2.2×10^{-3}
2.3	1.8×10^{-2}	4.9×10^{-2}	1.9×10^{-2}	4.9×10^{-2}
2.7	7.0×10^{-2}	0.223	7.1×10^{-2}	0.217
3.1	0.159	0.458	0.179	0.448

VI. CONCLUSION

This paper proposed an adaptive system to minimize the power consumption in LSAS systems. The adaptive system reduces the power consumption by combining ADTx with precoding selection and antenna optimization. The ADTx stage is responsible for dividing the transmission into L STs and selecting a suitable precoding technique per ST such that the total transmission time and latency are minimized. After ADTx, antenna array optimization is applied to further increase the duration of the hibernation period for a subset of antenna elements. The obtained analytical and simulation results showed that the proposed technique can provide EE improvements between 125% and 1124% in the suburban scenario, and between 196% and 952% in the rural scenario, without compromising QoS. It was also demonstrated that for rural environments with relatively smaller ISD values, the proposed technique can provide up to 500% power saving for fixed bit rate requirements.

APPENDIXES

APPENDIX I

CONTINUOUS TRANSMISSION RESOURCE ALLOCATION

For the sake of completeness, this section describes the continuous transmission scheme with bit rate and SINR adaptation. The adaptation is performed in two steps, which are the power control calculation and the RBs allocation. To maintain low complexity and delay, the continuous transmission scheme uses CJ precoding.

- *Power control calculation:*

The power control is applied if the achievable bit rate for all K UEs is less than the target bit rate. With $\mathcal{K}$ active users, the initial number of RBs per UE is given by $\mathcal{N}_{\text{in}}=\mathfrak{B}/\mathcal{K}$ and the initial throughput for all UEs is given by

$$\boldsymbol{R}_{\text{in}} = \{(\gamma_k, \mathcal{N}) \mid \mathcal{T}_{\text{D}}\mathcal{C}(\gamma_k, \mathcal{N}) \wedge k = 1, \ldots, K\} \quad (41)$$

where $\mathcal{C}$ is given by (7). The transmit power coefficient is given by

$$\varphi = \begin{cases} 1, & \mathfrak{D} = \varnothing \\ \max_{k=1,\ldots,K} \Theta_k, & \text{Otherwise} \end{cases} \quad (42)$$

where

$$\mathfrak{D} = \left\{\left(R_{\text{in},k}, R_k\right) \mid R_{\text{in},k} > R_k \wedge k = 1, \ldots, K\right\} \quad (43)$$

and $\boldsymbol{\Theta} \in \mathbb{R}^K$ is given by $\Theta_k = \gamma_{\text{target},k}/\gamma_k$, $k = 1, \ldots, K$, and $\boldsymbol{\gamma}_{\text{target}}$ is the target SINR, which is given by

$$\gamma_{\text{target},k} = \frac{\mathfrak{Z}_k\left(\Phi_k + \varrho_k + \Phi_k\varrho_k + 1\right)}{1 - \mathfrak{Z}_k}, \quad k = 1, \ldots, K.$$

$$\Phi_k = \frac{I_k}{\eta_k}$$
$$3_k = \frac{\mathcal{K}\left(2^{R_k T_{\text{fr}}/(\mathcal{N}_{\text{in}} QS)} - 1\right)}{(M-\mathcal{K})\,\varrho_k}. \tag{44}$$

As can be noted form (42), the power control is applied only when the achievable bit rate is lower than the throughput requirement.

- *RBs allocation*

After applying power control, further resource adjustment can be applied by considering the RB allocation. UEs that achieve more than the required bit rate can apply further reduction in the allocated RBs. This reduces the number of multiplexed UEs in some part of the RBs, hence, increases the achievable bit rate for the rest of UEs. The number of RBs for continuous transmission, $\boldsymbol{\mathcal{N}} \in \mathbb{R}^K$ is given by

$$\mathcal{N}_k = \frac{R_k T_{\text{fr}}}{\log_2\left(1+\gamma_{\varphi,k}\right)^Q}$$

such that $\sum_{k=1}^{K} \mathcal{N}_k \leq \mathcal{K}\mathfrak{B}$ and $\mathcal{N}_k \leq \mathfrak{B}$ for $k = 1, \ldots, K$, where $\boldsymbol{\gamma}_\varphi \in \mathbb{R}^K$ is the SINR coefficient with a power control coefficient φ. Using $\boldsymbol{\mathcal{N}}$, the RBs allocation $\boldsymbol{\mathcal{A}} \in \mathbb{R}^{K\times\mathfrak{B}}$, is given by

$$\mathcal{A}_{k,n} = \begin{cases} 1, & \text{allocate } k^{\text{th}} \text{ UE at the } n^{\text{th}} \text{ RB} \\ 0, & \text{otherwise} \end{cases} \tag{45}$$

subject to:

$$\sum_{n=1}^{\mathfrak{B}} \mathcal{A}_{k,n} = \mathcal{N}_k \tag{46a}$$
$$\mathcal{A}_n^{\Sigma} \leq \mathcal{K}_l,\ n = 1, \ldots, \mathfrak{B} \tag{46b}$$

where $\mathcal{A}_n^{\Sigma} = \sum_k^K \mathcal{A}_{k,n}$.

APPENDIX II
PROOF OF LEMMA 1

Given that the PDF of the distance, $f_D(d)$ between the MBS and EU is given by

$$f_D(d) = \begin{cases} \dfrac{2d}{d_{\max}^2}, & d \leq d_{\max} \\ 0, & \text{otherwise.} \end{cases} \tag{47}$$

By noting that $\alpha_{dB} = A + B\log(d)$, then $\alpha = 10^{\frac{A+B\log(d)}{10}}$. Substituting α in ψ gives

$$\psi = \frac{P_T}{\eta \times 10^{\frac{A+B\log(d)}{10}}} = \frac{P_T}{\eta \times 10^{\frac{A+B\log(d)}{10}}} = \frac{\varpi}{d^{\frac{B}{10}}}. \tag{48}$$

Because generally B is greater than 10, then ψ is strictly decreasing by increasing d. Therefore, the CDF of ψ is given by,

$$F_\psi(\psi) = P(d \leq u) = 1 - F_D(u) \tag{49}$$

where $F_D(d)$ is the CDF of d and $u = \left(\frac{\varpi}{\psi}\right)^{\frac{10}{B}}$. Consequently, $f_\psi(\psi)$ can be obtained using the chain rule,

$$f_\psi(\psi) = \frac{\partial}{\partial u}\left(1 - F_D(u)\right)\frac{\partial u}{\partial \psi} = -f_D(u)\frac{\partial u}{\partial \psi}. \tag{50}$$

By substituting $\frac{\partial u}{\partial \psi} = -\frac{10\left(\frac{\varpi}{\psi}\right)^{\frac{10}{B}}}{B\psi d_{\max}^2}$ and $f_D(u) = \frac{2}{d_{\max}^2}\left(\frac{\varpi}{\psi}\right)^{\frac{10}{B}}$ in (50) and simplifying the result, the PDF in (26) is obtained.

The CDF of the SINR is thus given by

$$\begin{aligned} F_\psi(\psi) &= \int_{\psi_{\min}}^{\psi} f_\psi(u)\,du \\ &= \frac{20}{d_{\max}^2 B}\int_{\psi_{\min}}^{\psi} \frac{1}{u}\left(\frac{\varpi}{u}\right)^{\frac{20}{B}} du \\ &= \frac{20}{d_{\max}^2 B}\varpi^{\frac{20}{B}}\int_{\psi_{\min}}^{\psi} \frac{1}{u^{\frac{20+B}{B}}} du \end{aligned} \tag{51}$$

Evaluating the integral gives

$$\int_{\psi_{\min}}^{\psi} \frac{1}{u^{\frac{20+B}{B}}} du = \frac{B}{20}\left(\psi_{\min}^{-\frac{20}{b}} - \psi^{-\frac{20}{b}}\right). \tag{52}$$

By substituting (52) in (51) we obtain

$$\begin{aligned} F_\psi(\psi) &= \frac{1}{d_{\max}^2}\varpi^{\frac{20}{B}}\left(\psi_{\min}^{-\frac{20}{B}} - \psi^{-\frac{20}{B}}\right) \\ &= \frac{1}{d_{\max}^2}\left[\left(\frac{\varpi}{\psi_{\min}}\right)^{\frac{20}{B}} - \left(\frac{1}{\psi^{\frac{20}{B}}}\right)^{\frac{20}{B}}\right]. \end{aligned} \tag{53}$$

REFERENCES

[1] Y. Hama and H. Ochiai, "Performance analysis of matched-filter detector for MIMO spatial multiplexing over Rayleigh fading channels with imperfect channel estimation," *IEEE Trans. Commun.*, vol. 67, no. 5, pp. 3220–3233, May 2019.
[2] *Technical Specification Group Services and System Aspects; Release 15*, Standard 3GPP TR 21.915 V15.0.0, 3rd Generation Partnership Project, Sep. 19, 2019.
[3] J. Hoydis, S. ten Brink, and M. Debbah, "Massive MIMO in the UL/DL of cellular networks: How many antennas do we need?" *IEEE J. Sel. Areas Commun.*, vol. 31, no. 2, pp. 160–171, Feb. 2013.
[4] H. Yang and T. L. Marzetta, "Performance of conjugate and zero-forcing beamforming in large-scale antenna systems," *IEEE J. Sel. Areas Commun.*, vol. 31, no. 2, pp. 172–179, Feb. 2013.
[5] W. Pramudito and E. Alsusa, "Confederation based RRM with proportional fairness for soft frequency reuse LTE networks," *IEEE Trans. Wireless Commun.*, vol. 13, no. 3, pp. 1703–1715, Mar. 2014.
[6] H. Quoc Ngo, E. G. Larsson, and T. L. Marzetta, "Energy and spectral efficiency of very large multiuser MIMO systems," *IEEE Trans. Commun.*, vol. 61, no. 4, pp. 1436–1449, Apr. 2013.
[7] K. Hinton, "Mobile communications WG architecture doc2: Update on modelling parameter," in *Proc. Internal Document GreenTouch Mobile Working Group*, Sep. 2014, pp. 5–12.
[8] D. Schoolar. *Massive MIMO Comes of Age: New Active Antenna Technologies Play a Major Role in the Evolution of Mobile Broadband Networks*. Accessed: Dec. 22, 2019. [Online]. Available: https://www.samsung.com/global/business/networks/products/radio-access/massive-mimo-unit/
[9] T. Klein, "Mobile communications WG architecture doc2: Reference scenarios," in *Proc. Internal Document GreenTouch Mobile Working Group*, Mar. 2013, pp. 10–21.

[10] *Cisco Visual Networking Index: Global Mobile Data Traffic Forecast Update, 2017–2022 White Paper*. Accessed: Dec. 22, 2019. [Online]. Available: https://www.cisco.com/c/en/us/solutions/collateral/service-provider/visual-networking-index-vni/white-paper-c11-738429.html

[11] *The Rise of Live Streaming*. Accessed: Dec. 22, 2019. [Online]. Available: https://www.ericsson.com/en/mobility-report/latest-social-media-trend-live-streaming

[12] P. Chang and G. Miao, "Optimal operation of base stations with deep sleep and discontinuous transmission," *IEEE Trans. Veh. Technol.*, vol. 67, no. 11, pp. 11113–11126, Nov. 2018.

[13] R. H. Etkin and E. Ordentlich, "The Degrees-of-Freedom of the K-user Gaussian interference channel is discontinuous at rational channel coefficients," *IEEE Trans. Inf. Theory*, vol. 55, no. 11, pp. 4932–4946, Nov. 2009.

[14] P. Frenger, P. Moberg, J. Malmodin, Y. Jading, and I. Godor, "Reducing energy consumption in LTE with cell DTX," in *Proc. IEEE 73rd Veh. Technol. Conf. (VTC Spring)*, May 2011, pp. 1–5.

[15] Q. Wang, F. Zhao, and T. Chen, "A base station DTX scheme for OFDMA cellular networks powered by the smart grid," *IEEE Access*, vol. 6, pp. 63442–63451, 2018.

[16] F. Parzysz and Y. Gourhant, "Drastic energy reduction with gDTX in low cost 5G networks," *IEEE Access*, vol. 6, pp. 58171–58181, 2018.

[17] X. Dong, F.-C. Zheng, X. Zhu, and J. Luo, "HetNets with range expansion: Local delay and energy efficiency optimization," *IEEE Trans. Veh. Technol.*, vol. 68, no. 6, pp. 6147–6150, Jun. 2019.

[18] J.-F. Cheng, H. Koorapaty, P. Frenger, D. Larsson, and S. Falahati, "Energy efficiency performance of LTE dynamic base station downlink DTX operation," in *Proc. IEEE 79th Veh. Technol. Conf. (VTC Spring)*, May 2014, pp. 1–5.

[19] K. Adachi, J. Joung, S. Sun, and P. Hui Tan, "Adaptive coordinated napping (CoNap) for energy saving in wireless networks," *IEEE Trans. Wireless Commun.*, vol. 12, no. 11, pp. 5656–5667, Nov. 2013.

[20] Y. Cui, V. K. N. Lau, and Y. Wu, "Delay-aware BS discontinuous transmission control and user scheduling for energy harvesting downlink coordinated MIMO systems," *IEEE Trans. Signal Process.*, vol. 60, no. 7, pp. 3786–3795, Jul. 2012.

[21] J. Joung, Y. K. Chia, and S. Sun, "Energy-efficient, large-scale distributed-antenna system (L-DAS) for multiple users," *IEEE J. Sel. Topics Signal Process.*, vol. 8, no. 5, pp. 954–965, Oct. 2014.

[22] F. Tan, T. Lv, and S. Yang, "Power allocation optimization for energy-efficient massive MIMO aided multi-pair Decode-and-Forward relay systems," *IEEE Trans. Commun.*, vol. 65, no. 6, pp. 2368–2381, Jun. 2017.

[23] W. Dinkelbach, "On nonlinear fractional programming," *Manage. Sci.*, vol. 13, no. 7, pp. 492–498, Mar. 1967. [Online]. Available: http://www.jstor.org/stable/2627691

[24] F. Fang, H. Zhang, J. Cheng, S. Roy, and V. C. M. Leung, "Joint user scheduling and power allocation optimization for energy-efficient NOMA systems with imperfect CSI," *IEEE J. Sel. Areas Commun.*, vol. 35, no. 12, pp. 2874–2885, Dec. 2017.

[25] L. Sboui, Z. Rezki, and M.-S. Alouini, "Energy-efficient power allocation for MIMO-SVD systems," *IEEE Access*, vol. 5, pp. 9774–9784, 2017.

[26] P. Kou, X. Li, R. Guo, and Y. Hei, "Ergodic capacity-based energy optimization algorithm in massive MIMO systems," in *Proc. Int. Conf. Comput., Netw. Commun. (ICNC)*, Kauai, HI, USA, Feb. 2016, pp. 1–5.

[27] S. D'Oro, A. Zappone, S. Palazzo, and M. Lops, "A learning approach for low-complexity optimization of energy efficiency in multicarrier wireless networks," *IEEE Trans. Wireless Commun.*, vol. 17, no. 5, pp. 3226–3241, May 2018.

[28] Y. Lin, Y. Wang, C. Li, Y. Huang, and L. Yang, "Joint design of user association and power allocation with proportional fairness in massive MIMO HetNets," *IEEE Access*, vol. 5, pp. 6560–6569, 2017.

[29] T. Van Chien, E. Bjornson, and E. G. Larsson, "Joint power allocation and user association optimization for massive MIMO systems," *IEEE Trans. Wireless Commun.*, vol. 15, no. 9, pp. 6384–6399, Sep. 2016.

[30] W. Pramudito, E. Alsusa, D. K. C. So, and K. A. Hamdi, "Load aware adaptive scheduling for energy efficient suburban massive MIMO networks," in *Proc. IEEE Global Commun. Conf. (GLOBECOM)*, San Diego, CA, USA, Dec. 2015, pp. 1–6.

[31] W. Pramudito, E. Alsusa, D. K. C. So, and K. A. Hamdi, "Joint successive DTx and antenna optimization for energy efficient large scale antenna systems," in *Proc. IEEE Global Commun. Conf. (GLOBECOM)*, Dec. 2015, pp. 1–6.

[32] W. Pramudito, E. Alsusa, D. K. C. So, and K. A. Hamdi, "Adaptive LSAS transmission for energy optimisation in low density cellular networks," in *Proc. IEEE Online Conf. Green Commun. (OnlineGreenComm)*, Nov. 2014, pp. 1–6.

[33] J. Proakis and M. Salehi, *Digital Communication*, 5th ed. New York, NY, USA: McGraw-Hil, 2008.

[34] G. Caire and S. Shamai, "On the achievable throughput of a multiantenna Gaussian broadcast channel," *IEEE Trans. Inf. Theory*, vol. 49, no. 7, pp. 1691–1706, Jul. 2003.

[35] L. Thomas Marzetta, G. Erik Larsson, H. Yang, and H. Q. Ngo, *Fundamentals Massive MIMO*. Cambridge, U.K.: Cambridge Univ. Press, Nov. 2016.

[36] H. Yang and T. L. Marzetta, "Total energy efficiency of cellular large scale antenna system multiple access mobile networks," in *Proc. IEEE Online Conf. Green Commun. (OnlineGreenComm)*, Oct. 2013, pp. 27–32.

[37] T. L. Marzetta, "How much training is required for multiuser MIMO?" in *Proc. 40th Asilomar Conf. Signals, Syst. Comput.*, Nov. 2006, pp. 359–363.

[38] C. Desset, B. Debaillie, V. Giannini, A. Fehske, G. Auer, H. Holtkamp, W. Wajda, D. Sabella, F. Richter, M. J. Gonzalez, H. Klessig, I. Godor, M. Olsson, M. A. Imran, A. Ambrosy, and O. Blume, "Flexible power modeling of LTE base stations," in *Proc. IEEE Wireless Commun. Netw. Conf. (WCNC)*, Apr. 2012, pp. 2858–2862.

[39] C. Desset, B. Debaillie, and F. Louagie, "Towards a flexible and future-proof power model for cellular base stations," in *Proc. 24th Tyrrhenian Int. Workshop Digit. Commun. Green ICT (TIWDC)*, Sep. 2013, pp. 1–6.

[40] Y. Qi, M. Hunukumbure, M. Nekovee, J. Lorca, and V. Sgardoni, "Quantifying data rate and bandwidth requirements for immersive 5G experience," in *Proc. IEEE Int. Conf. Commun. Workshops (ICC)*, May 2016, pp. 455–461.

[41] C. Shephard, H. Yu, N. Anand, E. Li, T. Marzetta, R. Yang, and L. Zhong, "Argos: Practical many-antenna base stations," in *Proc. ACM Int. Conf. Mobile Comput. Netw. (MobiCom)*, Aug. 2012, pp. 53–64.

[42] H. A. David and H. N. Nagaraja, "Order statistics," in *Order Statistics., Wiley Series in Probability and Statistics*. Hoboken, NJ, USA: Wiley, 2003.

[43] G. Louth, "Consultation on assessment of future mobile competition and proposals for the award of 800 MHz and 2.6 GHz spectrum and related issues," OFCOM, London, U.K., Tech. Rep. 1, Mar. 2011.

WAHYU PRAMUDITO (Member, IEEE) received the B.Eng. degree in computing and communication systems engineering and the Ph.D. degree in electrical and electronic engineering from the University of Manchester, Manchester, U.K., in 2009 and 2013, respectively. He is currently a Research Associate with the Microwave and Communications Systems Group, School of Electrical and Electronic Engineering, University of Manchester. His research interests are in the area of communication theory and its applications, particularly in interference management techniques for heterogeneous cellular networks, green communication networks, multiantenna systems, and cooperative communication systems.

EMAD ALSUSA (Senior Member, IEEE) received the Ph.D. degree in telecommunications from the University of Bath, U.K., in 2000. He was appointed to work on developing high data rates systems as part of an Industrial Project based with Edinburgh University, in 2000. He joined Manchester University (then UMIST), in September 2003, as a Faculty Member, where his current rank is a Reader in the Communication Engineering Group. His research interests include the area of communication systems with a focus on Physical, MAC and network layers including developing techniques and algorithms for array signal detection, channel estimation and equalization, adaptive signal precoding, interference avoidance through novel radio resource management techniques, cognitive radio and energy and spectrum optimization techniques. Applications of his research include cellular networks, the IoT and powerline communications. His research work has resulted in over 200 journals and refereed conference publications mainly in top IEEE transactions and conferences. He has supervised over 20 PhDs to successful completion and currently responsible for several more. Dr. Alsusa is a Fellow of the UK Higher Academy of Education He was the TPC Track Chair of a number of conferences such as VTC'16, GISN'16, PIMRC'17, and Globecom'18, as well as the General Co-Chair of the OnlineGreenCom'16 Conference. He is currently the U.K. Representative in the International Union of Radio Science. He has received a number of awards including the Best Paper Award in the International Symposium on Power Line Communications 2016 and the Wireless Communications and Networks Conference 2019.

ARAFAT AL-DWEIK (Senior Member, IEEE) received the M.S. *(Summa Cum Laude)* and Ph.D. *(Magna Cum Laude)* degrees in electrical engineering from Cleveland State University, Cleveland, OH, USA, in 1998 and 2001, respectively. He was with Efficient Channel Coding, Inc., Cleveland, from 1999 to 2001. From 2001 to 2003, he was the Head of Department of Information Technology with the Arab American University, Palestine. Since 2003, he has been with the Department of Electrical Engineering, Khalifa University, UAE. He joined the University of Guelph, ON, Canada, as an Associate Professor from 2013 to 2014. He is currently a Visiting Research Fellow with the School of Electrical, Electronic and Computer Engineering, Newcastle University, Newcastle upon Tyne, U.K. He is also a Research Professor with Western University, London, ON, Canada, and University of Guelph. Dr. Al-Dweik has extensive editorial experience where he served as an Associate Editor for the IEEE Transactions on Vehicular Technology and the *IET Communications*. He has extensive research experience in various areas of wireless communications that include modulation techniques, channel modeling and characterization, synchronization and channel estimation techniques, OFDM technology, error detection and correction techniques, MIMO, and resource allocation for wireless networks. He is a member of Tau Beta Pi and Eta Kappa Nu. He received the Fulbright Scholarship, from 1997 to 1999, the Hijjawi Award for Applied Sciences, in 2003, and the Fulbright Alumni Development Grant, in 2003 and 2005, and the Dubai Award for Sustainable Transportation in 2016, and the Leader-Founder Reserch Award, in 2019. He is a Registered Professional Engineer in the Province of Ontario, Canada.

KHAIRI A. HAMDI (Senior Member, IEEE) received the B.Sc. degree in electrical engineering from Alfateh University, Tripoli, Libya, in 1981, the M.Sc. degree (Hons.) from the Technical University of Budapest, Budapest, Hungary, in 1988, and the Ph.D. degree in telecommunication engineering from the Hungarian Academy of Sciences, Budapest, in 1993. Previously, he held research and academic posts with the Department of Computer Science, The University of Manchester, and the Department of Electronic Systems Engineering, University of Essex. He was a BT Research Fellow in summer 2002, and was a Visiting Assistant Professor with Stanford University during the academic year 2007 to 2008. He is currently a Senior Lecturer with The University of Manchester. His current research interests include modeling and performance analysis of wireless communication systems, and networks.

DANIEL K. C. SO (Senior Member, IEEE) received the B.Eng. (Hons) degree in electrical and electronics engineering from the University of Auckland, Auckland, New Zealand, in 1996, and the Ph.D. degree in electrical and electronics engineering from the Hong Kong University of Science and Technology (HKUST), in 2003. From 1997 to 1998, he was a Senior Software Engineer with Orion Health, Auckland, New Zealand. He was a Lecturer with the University of Manchester, in 2003, where he is currently a Reader and Discipline Head of Education with the Department of Electrical and Electronic Engineering. His research interests include green communications, NOMA, 5G networks, heterogeneous networks, cognitive radio, massive MIMO, D2D communications, cooperative MIMO schemes, multihop communication, channel equalization, and estimation techniques. He served as a Symposium Co-Chair of the IEEE ICC 2019 and Globecom 2020, and the Track Co-Chair for the IEEE Vehicular Technology Conference (VTC) Spring 2016, 2017, and 2018. He is currently an Editor for the IEEE Transactions on Wireless Communications and the IEEE Wireless Communication Letters.

THOMAS L. MARZETTA (Life Fellow, IEEE) was born in Washington, D.C. He received the Ph.D. degree in electrical engineering from the Massachusetts Institute of Technology, in 1978. His dissertation extended, to two dimensions, the three-way equivalence of autocorrelation sequences, minimum-phase prediction error filters, and reflection coefficient sequences. He worked for Schlumberger-Doll Research from 1978 to 1987 to modernize geophysical signal processing for petroleum exploration. He was the Head of group with Nichols Research Corporation from 1987 to 1995 which improved automatic target recognition, radar signal processing, and video motion detection. He joined Bell Laboratories, in 1995 (formerly part of AT&T, then Lucent Technologies, now Alcatel-Lucent). He has had research supervisory responsibilities in communication theory, statistics, and signal processing. He specializes in multiple-antenna wireless, with a particular emphasis on the acquisition and exploitation of channel-state information. He is the Originator of Large-Scale Antenna Systems. Dr. Marzetta was a recipient of the 1981 ASSP Paper Award from the IEEE Signal Processing Society. He was an Associate Editor for the IEEE Transactions on Signal Processing, and for the IEEE Transactions on Image Processing, and a Guest Associate Editor for the IEEE Transactions on Information Theory Special Issue on Signal Processing Techniques for Space-Time Coded Transmissions (October 2002) and for the IEEE Transactions on Information Theory Special Issue on Space-Time Transmission, Reception, Coding, and Signal Design (October 2003).